Numerical Testbench for A Priori Uncertainty Estimation of Dielectric Spectroscopy in Organ-On-Chip Devices

Hosman, T. B.; Shokrolahzade, E.; Mastrangeli, M.; Spirito, M.

DOI
10.1109/IMS40360.2025.11103818

Publication date
2025

Document Version
Final published version

Published in
2025 IEEE/MTT-S International Microwave Symposium, IMS 2025

Numerical Testbench for *A Priori* Uncertainty Estimation of Dielectric Spectroscopy in Organ-on-Chip Devices

T.B. Hosman*, E. Shokrolahzade*, M. Mastrangeli, M. Spirito
Department of Microelectronics, Delft University of Technology, The Netherlands
{t.b.hosman, e.shokrolahzade, m.mastrangeli, m.spirito}@tudelft.nl

***Abstract*—In this work, we present a numerical testbench, realized in a circuit simulation environment, enabling a priori uncertainty evaluation of dielectric spectroscopy in the application field of organs-on-chip. This testbench evaluates the impact of noise, ambient temperature variation and impurity of liquid standards on the uncertainty of dielectric spectroscopy measurements. Moreover, the proposed approach allows to account for the impact on measurement sensitivity of system parameters such as probe dimensions and probe coatings. The estimated uncertainty contributions for the considered effects are compared and benchmarked experimentally. Finally, the testbench is employed to project the dielectric spectroscopy accuracy on a relevant biological application, namely monitoring the growth of a 7 μm-thick kidney cell monolayer.**

***Keywords*—biological systems, biological tissues, circuit simulation, coaxial cables, dielectric measurement, error analysis, measurement uncertainty, organ-on-chip, reflectometry.**

I. Introduction

Organ-on-chip (OoC) technology has recently emerged to overcome several limitations of the current drug development process, aiming for accurate in-vitro models of human organs [1]. OoC models could be applied in pre-clinical drug testing, developing personalised medicine, and reducing the need for ethically-debatable animal-based drug studies [2]. Integrated sensing is crucial for the success of OoC technology, as it provides insight into tissue's physiological state and can be used to correlate its changes during drug exposure with relevant biological endpoints. Consequently, time-continuous non-invasive sensing has been identified as a main unmet need in OoC applications [3]. Dielectric spectroscopy (DS) using open-ended coaxial probes (OECPs) has been proposed as a fitting sensing solution for OoC [4]. However, since tissue dynamics ought to be monitored with OECPs, understanding the impact of various uncertainty contributors and identifying eventual bottlenecks before building a setup aid in optimising the practical setup design process. This is particularly relevant when such effects are further confounded by intermediate components such as interconnects, biocompatible surface coatings and calibration.

In this work, after introducing the experimental OECP-centred DS setup (Section II), we present the proposed numerical testbench enabling the *a priori* determination of uncertainty contributors. Vector network analyser (VNA) noise, calibration liquid purity and ambient temperature offset are the different error contributors considered in this study and they are characterised and embedded in the testbench based on measurement and simulation (Section III). The impact of interconnect, surface coating and probe size on a DS measurement is included, resulting in a detailed overview of individual error contributors (Section IV). After validation, the technique is exploited for a case study to identify whether growth-stage monitoring of 7 µm-thick kidney cell cultures is a technically-feasible sensing application for DS (Section V).

II. Dielectric Spectroscopy using OECPs

The dielectric response of a sample to an applied electric field can be obtained by measuring the reflection coefficient Γ. The setup employed in this work uses a three Γ calibration (often denoted as SOL in the coaxial domain) by employing three different media (i.e. water, air, and methanol). An iterative inversion algorithm uses a numerical OECP model to convert the reflection coefficient (Γ) of a material under test (MUT) to a dielectric spectrum [4] [5]. In this work, ethanol is used as MUT for the uncertainty analysis since ethanol has a dielectric spectrum similar to (breast) tissue [6].

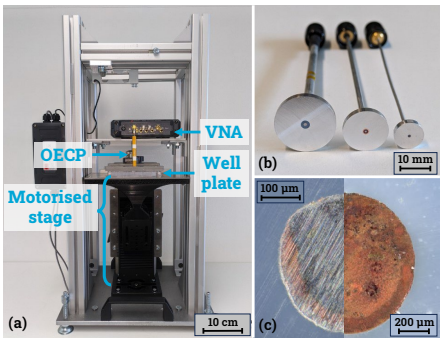

Fig. 1: (a) overview of the DS measurement setup; (b) custom OECPs without stiffener; (c) Surface of heavily used OECPs with (left) and without (right) coating. The coated probe is pristine while the uncoated probe is corroded.

The setup used in this work for DS measurements is shown in Fig. 1a. The OECP (Fig. 1b) is connected to a VNA (Keysight P9374A) via a 90° elbow connector, thus avoiding the usage of a flexible cable, which is prone to phase fluctuation during measurements. The probe is strengthened with a 3D-printed stiffener to reduce measurement errors due to bending and vibrations. Samples are positioned using a motorised stage. The VNA's reflectometry data is collected on a computer for post-processing. Frequency sweeps from 50 MHz to 20 GHz with an intermediate frequency bandwidth (IFBW) of 100 Hz at a power source level of 0 dBm are performed. The used power level, considering the reflection

* equal contribution

2025 IEEE/MTT-S International Microwave Symposium - IMS 2025 | 979-8-3315-1409-9/25/$31.00 ©2025 IEEE | DOI: 10.1109/IMS40360.2025.11103818

coefficient of the mentioned MUT, translates into around $-7\ dBm$ of absorbed power at $10\ GHz$.

A biocompatible coating is required to shield the biological sample from invasive and potentially-toxic materials (ensuring the OoC's physiological relevance) and protect the sensor surface from degrading over time (Fig. 1c shows heavy corrosion in long-term use if a coating is not applied).

Three variations of the OECP were manufactured in-house using $50\ \Omega$ semi-rigid coaxial cables from Pasternack (Fig. 1b) according to a custom fabrication protocol (including flange adaptation and surface polishing) and are referred to in this work by the diameter of the inner coaxial conductor ($0.28\ mm$, $0.51\ mm$ and $0.91\ mm$, respectively) [7] [8] [9]. Two protocols for biocompatible probe coating were used: 1) a polydimethylsiloxane (PDMS) moulding process, depositing a PDMS layer on top of the sensing surface and limited to a thickness of $110\ \mu m$, and 2) a Parylene C vapour deposition process using a remote reactor deposition system (SCS PDS 2010), depositing a conformal layer of $2.0\ \mu m$ thickness. PDMS and Parylene C have an estimated dielectric permittivity of 2.6 and 3.1, respectively [10] [11]. The probes and their coated variations have been simulated in CST Studio Suite to extract their scattering parameter response. This was used to model the probes in the numerical uncertainty simulation environment.

III. Numerical Uncertainty Estimation

In RF metrology, uncertainty estimation is usually calculated after conducting measurements on a given setup [12]. However, to design a setup capable of measuring diverse dielectric spectra of tissue [13] with enough sensitivity, it is necessary to know the expected uncertainty of the setup in advance. For this purpose, we propose a testbench realised in the Keysight ADS environment to accurately replicate the measurement setup. The mapping of lab-specific systematic errors and the inclusion of MonteCarlo perturbations, based on real-life values, allows for the generation of uncertainty bounds using the simulation environment. The testbench includes the following uncertainty sources: VNA noise [14], standard temperature offset and standard purity offset. The real-life VNA error terms are included in the testbench to provide the accurate level of systematic error in the SOL calibration, which is required for the correct scaling of the VNA noise level. The temperature offset is caused by a mismatch between the ambient temperature and the temperature assumed in the model used for calibration [15] [16]. Similarly, purity offset is caused by a mismatch in model-assumed and actual purity of the liquid standards. In this work, to simplify the modelling of permittivity, only the primary impurity found in the literature is considered. For methanol (load), the main impurity is water [17], while water's (short) main impurity is salinity [18] [19]. Air (open) is always treated as ideal in this study. For mixing, a percentual average of dielectric spectra is used according to equation 1, where P is the purity of the calibration liquid:

$$\varepsilon^*_{impure} = P \cdot \varepsilon^*_{pure} + (1-P) \cdot \varepsilon^*_{impurity} \quad (1)$$

The testbench for numerical uncertainty estimation consists of the nominal S-parameters of all components in the setup, i.e. VNA error terms, coaxial interconnects, and the probes. Each component was characterised through a separate measurement, except for the probe response, which is obtained via a 3D simulation.

Fig. 2 shows the VNA model used to collect the data of the incident and reflected waves. The noise of a VNA is characterised according to the guidelines of reference [20] (at $0\ dBm$ power and $100\ Hz$ IFBW) and it is then applied to the incident and reflected wave at the VNA's equivalent internal receiver ($50\ \Omega$ resistors in Fig. 2). From this setup noisy S-parameters are calculated in a MonteCarlo simulation. These results approximately follow those of state-of-the-art post-measurement uncertainty calculating solutions like METAS VNATools [12]. The procedure for temperature and impurity study is a simple replacement of the standard responses with the non-ideal case, as explained in Section IV.C.

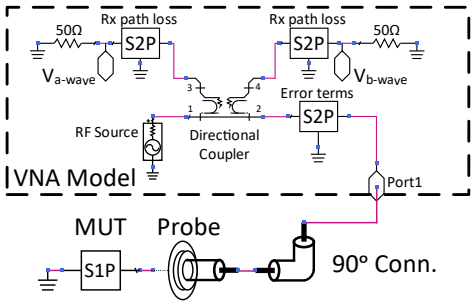

Fig. 2: Schematic of numerical uncertainty evaluation testbench in ADS.

IV. Model Description and Validation

A. Uncertainty Estimation for Probe Size and Coatings

Models of all OECPs with three coating variations (uncoated, $110\ \mu m$ PDMS and $2.0\ \mu m$ Parylene C) were simulated using CST Studio Suite. The $0.28\ mm$ probe's transmission coefficient can be seen in Fig. 3. The response of the uncoated probe shows the highest transmission coefficient for this particular device, as it is not impeded by any intermediate material. In comparison, the PDMS-coated probe shows a significant dip in the transmission of around $20\ dB$ at lower frequencies, indicating a significant performance degradation. The thinly-coated Parylene C probe recovers most of the probe's transmission capability. Especially at higher frequencies, this probe performs similarly to an uncoated probe.

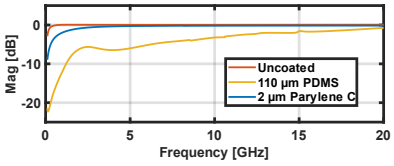

Fig. 3: Comparison of transmission coefficient magnitude of $0.28\ mm$ probes with different surface coatings.

The probe's transmission and reflection coefficients were used in the numerical model to estimate the S_{11} uncertainty of DS for different probe sizes. The DS standard deviation for

the different 0.28 mm probes can be found in Fig. 4. The results show a significantly higher standard deviation for the PDMS-coated probe. Since the use of the uncoated probe with biological samples is not desired, the remainder of this paper focuses on Parylene C-coated probes.

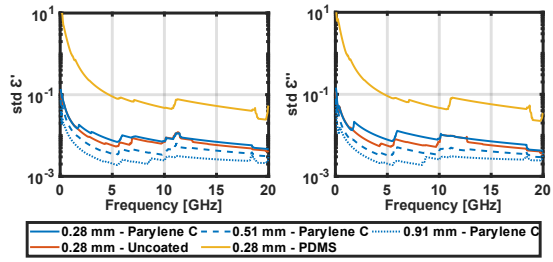

Fig. 4: Numerically-evaluated 3σ standard deviation of ethanol's complex permittivity due to VNA noise, with varying probe dimensions (0.28 mm, 0.51 mm and 0.91 mm) indicated by blue lines and varying coatings (uncoated, 110 μm PDMS, 2.0 μm Parylene C) indicated by solid lines.

Using the same approach described in the previous section, uncertainty due to VNA noise for different probe sizes was estimated using CST simulations of Parylene C-coated 0.28 mm, 0.51 mm and 0.91 mm probes, and analysed using the numerical testbench. A trend can be seen where larger probes reduce VNA noise (Fig. 4). However, probe size is also proportional to sensing depth [5], so larger probes are not necessarily preferred. In fact, the 0.28 mm probe has a sensing depth below 1.5 mm through water [4], which fittingly confines the sensing volume to the layers of interest in the micro-scale domain of OoC devices (PBS, cells and PC, see Section V). As such, further analysis in this work focuses on the 0.28 mm probe.

B. Uncertainty Estimation for Purity and Temperature

To assess the effect of ambient temperature and calibration liquid purity, the responses of each liquid standard were modelled at temperature offsets of $\pm 0.5\,°C$ and $\pm 1\,°C$ and purity levels of 99 % , 99.9 % and 99.99 % . For the calibrations with temperature offset, all calibration liquids are assumed to suffer from the same offset. For purity mismatch, four combinations of short and load standards, both impure and pure, were used in the testbench to find the maximum error on the complex permittivity.

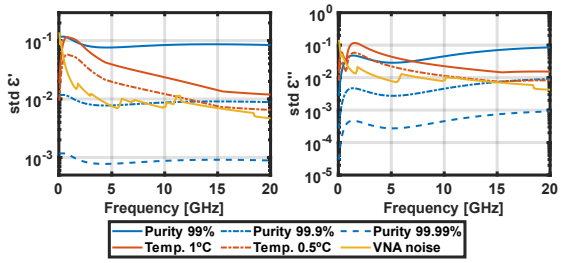

Fig. 5: Numerically-evaluated 3σ standard deviation of ethanol's complex permittivity using Parylene C-coated 0.28 mm probes shown as a function of calibration liquid purity (blue lines), ambient temperature (red lines) and VNA noise (yellow line).

Fig. 5 shows that, for the chosen settings of VNA, purity generally does not contribute to the total error when high purities are used. Since error contribution caused by temperature control is comparable to purity in higher frequencies and at least one order of magnitude higher in lower frequencies, temperature control of the samples is the leading contributor if the sample purities are better than 99.9%.

C. Validation With Experimental Data

A comparative analysis was conducted to validate the uncertainty estimation presented. For each standard the pure and impure (99 %) version was measured at two different lab temperatures ($T \approx 21\,°C$ and $T \approx 22\,°C$) and PBS was used as MUT. PBS was opted for validation as it was available in-house with well-known purity while remaining biologically relevant. The measurements were compared to compound uncertainties of VNA noise, 99 % purity and $+1\,°C$ temperature difference, and in Fig. 6, the difference of permittivity is shown with respect to the mean of measurements, it can be seen that the (3σ) predicted bound closely confines all the conducted validation data, thus proving that the presented model is an accurate and reliable *a priori* estimator for DS measurements. It is noteworthy that the testbench provides a numerical approximation of the uncertainties, and accurate values should be calculated post-measurement using a classical approach.

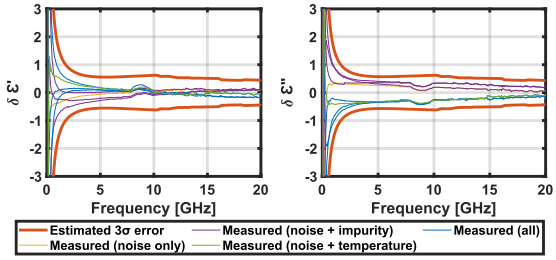

Fig. 6: Estimated (3σ) error for PBS's complex permittivity error assuming 99 % purity, $\pm 0.5\,°C$ temperature difference (around 21.5 °C) and VNA noise (in red), compared to measured errors due to noise (in yellow), impurity (in purple), temperature (in green) and a combination of all errors (in blue).

V. Case Study on Kidney Monolayer Confluency

To fully appreciate the value of the testbench for OoC applications, a case study was conducted where the growth stage of a kidney cell monolayer is monitored. Here, a polycarbonate (PC) well plate, in which cells are conventionally cultured, is modelled in CST for two edge cases. The first case assumes the well plate before seeding cells (Fig. 7a), where cell culturing medium (a mix of saline and proteins) is modelled as phosphate-buffered saline (PBS).

The second case assumes the final growth stage (Fig. 7b) where kidney cells have grown a confluent layer on top of the PC surface. Kidney cells are chosen because they naturally grow as a uniform monolayer of about 7 μm thick, making them easier to model and measure [6] [21]. Since the cell layer is relatively very thin, the change in permittivity of the two cases will be small and should be compared to the expected uncertainty of the testbench to predict whether cell layer growth can be measured.

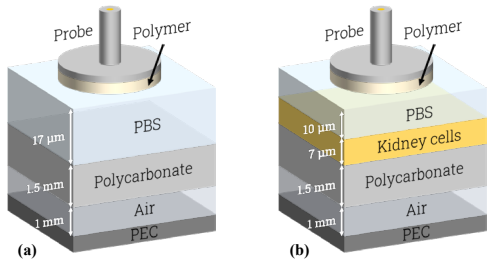

Fig. 7: Material composition of OoC case-study. (a) Single well (of well plate) with fully-grown layer of kidney cells, (b) Single well before cell seeding.

For this case study, the testbench employs a $0.28\,mm$ Parylene C-coated probe with a temperature tolerance of $\pm 0.5\,°C$, a 99.9 % purity for water (short), a 99.99 % purity for methanol (load) and VNA noise. Fig. 8 shows the difference between the expected permittivity delta due to cell growth, and the estimated uncertainty. On average, the estimated error is more than 14 times lower than the expected response, indicating excellent resolution to monitor monolayer cell growth over time (i.e. different growth stages with different cell densities). It should be noted that ε'' is coinciding around $2.2\,GHz$ for the two simulated cases, thus creating a singularity for the plotted delta ε''.

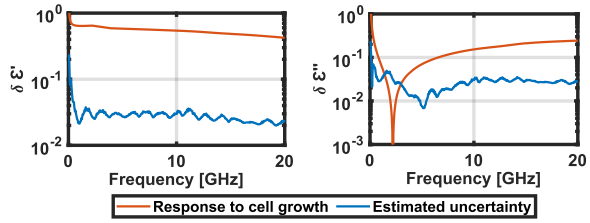

Fig. 8: Simulated complex permittivity delta due to the growth of a 7 μm-thick kidney cell layer (red line) versus the estimated 3σ standard deviation considering noise, temperature and purity.

VI. Conclusion

This paper presented a testbench for the *a priori* estimation of DS measurement uncertainty due to VNA noise, calibration liquid temperature and impurity, while also considering all system components such as interconnects, probe size and probe surface coating, and calibration. This was used to decide on probe size, where there is a trade-off in which larger probes are less influenced by VNA noise, but have lower spatial resolution (i.e. larger sensing volume). The results also show that thin Parylene C coatings can be used in DS with nearly-negligible compromise for biocompatible OoC applications.

The relative contributions estimated via the testbench allow for case-to-case consideration of error sources essential for building a DS setup. The testbench shows excellent correspondence with experimental data in which noise, temperature and purity were all varied. Therefore, it was used to predict whether DS is capable of sensing the growth of 7 μm-thick kidney cell monolayers. On average, the estimated error is over 14 times lower than required. This makes DS not just sensitive enough to measure the presence of a cell monolayer, but also to monitor various intermediate growth stages.

References

[1] D. M. Nahon et al., "Standardizing designed and emergent quantitative features in microphysiological systems," Nature Biomedical Engineering, pp. 1–22, Aug. 2024.

[2] L. A. Low, C. Mummery, B. R. Berridge, C. P. Austin and D. A. Tagle, "Organs-on-chips: into the next decade," Nature Reviews Drug Discovery, vol. 20, no. 5, pp. 345-361, 2021.

[3] M. Mastrangeli and J. van den Eijnden-van Raaij, "Organs-on-chip: The way forward," Stem Cell Reports, vol. 16, no. 9, pp. 2037-2043, 2021.

[4] T. B. Hosman, M. Mastrangeli and M. Spirito, "Non-contact Dielectric Spectroscopy of Multi-Layered Substrates: Towards Organ-on-Chip Applications," IEEE J-ERM, Jan. 2025, doi: https://doi.org/10.1109/jerm.2025.3538953.

[5] H. T. Shivamurthy, "On the Design and Analysis of Micro-metric Resolution Arrays in Integrated Technology for Near-Field Dielectric Spectroscopy," Ph.D. thesis, Delft University Of Technology, Delft, The Netherlands, 2020.

[6] S. Gabriel, Ed., "Modelling the frequency dependence of the dielectric properties to a 4 dispersions spectrum," Nov. 06, 1997. Available: http://niremf.ifac.cnr.it/docs/DIELECTRIC/AppendixC.html

[7] Pasternack Enterprises Inc, "047 Semi-rigid Coax Cable with Tinned Aluminum Outer Conductor," https://www.pasternack.com/images/ProductPDF/PE-SR047ALSTRAIGHT.pdf, 2023 (accessed: 15/01/2024).

[8] Pasternack Enterprises Inc, "086 Semi-rigid Coax Cable with Tinned Aluminum Outer Conductor," https://www.pasternack.com/images/ProductPDF/PE-SR405AL-STRAIGHT.pdf, 2023 (accessed: 16/01/2024).

[9] Pasternack Enterprises Inc, "141 Semi-rigid Coax Cable with Tinned Aluminum Outer Conductor," https://www.pasternack.com/images/ProductPDF/PE-SR402AL-STRAIGHT.pdf, 2023 (accessed: 16/01/2024).

[10] H. Shivashankar, A. M. Kevin, S. B. S. Manohar, and S. M. Kulkarni, "Investigation on dielectric properties of PDMS based nanocomposites," Physica B: Condensed Matter, vol. 602, pp. 412357–412357, Feb. 2021.

[11] Vertical Solutions Inc., "The Complete Guide To Parylene Coatings," [Online]. Available: https://vsiparylene.com/parylene-properties/. [Accessed 6 March 2024].

[12] M. Wollensack, J. Hoffmann, J. Ruefenacht and M. Zeier, "VNA Tools II: S-parameter uncertainty calculation," in 79th ARFTG Microwave Measurement Conference, Montreal, QC, Canada, 2012.

[13] R. K. Foster and H. P. Schwann, "Dielectric properties of tissues and biological materials: A critical review," Critical Reviews in Biomedical Engineering, vol. 17, no. 1, pp. 25-104, 1989.

[14] F. A. Mubarak, R. Romano, L. Galatro, V. Mascolo, G. Rietveld and M. Spirito, "Noise Behavior and Implementation of Interferometer-Based Broadband VNA," IEEE Transactions on Microwave Theory and Techniques, vol. 67, no. 1, pp. 249-260, 2019.

[15] B. Jordan, R. J. Sheppard, and S Szwarnowski, "The dielectric properties of formamide, ethanediol and methanol," Journal of Physics D, vol. 11, no. 5, pp. 695–701, Apr. 1978.

[16] P. Petong, R. Pottel, and U. Kaatze, "Water−Ethanol Mixtures at Different Compositions and Temperatures. A Dieletric Relaxation Study," The Journal of Physical Chemistry A, vol. 104, no. 32, pp. 7420–7428, Aug. 2000.

[17] "Methanol CHROMASOLV certificate of analysis," Honeywell Specialty Chemicals GmbH, Seelze, Germany.

[18] U. Kaatze, "Complex permittivity of water as a function of frequency and temperature," Journal of Chemical and Engineering Data, vol. 34, no. 4, pp. 371–374, Oct. 1989.

[19] A. Peyman, C. Gabriel, and E. H. Grant, "Complex permittivity of sodium chloride solutions at microwave frequencies," Bioelectromagnetics, vol. 28, no. 4, pp. 264–274, 2007.

[20] M. Zeier, D. Allal, and R. Judaschke. "Guidelines on the evaluation of vector network analysers (VNA)." EURAMET Calibration Guide 3.12 (2018): 507-521.

[21] S. M. Zehnder, M. Suaris, M. M. Bellaire, and T. E. Angelini, "Cell Volume Fluctuations in MDCK Monolayers," Biophysical Journal, vol. 108, no. 2, pp. 247–250, Jan. 2015.